3D-Printed Electrochemical Cell for *In Situ* Analysis

Thesis

Completed in Partial Fulfillment of the Requirements for Graduation with Honors Research Distinction in the Department of Mechanical and Aerospace Engineering at The Ohio State University

By

Dustin T. Goetz

Undergraduate Program in Mechanical Engineering

The Ohio State University

2020

Thesis Committee

Vicky Doan-Nguyen, Ph.D., Advisor

Jung-Hyun Kim, Ph.D.

Abstract

Electrochemical storage systems, such as batteries, are essential for mobile systems and for matching the time-varying energy demands of consumers on renewable energy grids. *In situ* analysis allows researchers to observe the electrochemical mechanisms of the components of batteries in real time which can inform the development of next-generation battery materials. Unfortunately, there is no standard cell for holding battery components during *in situ* analyses, leading to non-standardized results across labs. Although there are commercial *in situ* cells and individual labs have designed their own *in situ* cells, factors such as cost, experimental conditions, equipment specifications, and lack of quality control have prevented the adaptation of a single *in situ* design. In this study, we introduce a novel approach that leverages advancements in additive manufacturing to create a cell entirely from 3D-printed components and common commercial parts. This "3D-printed *in situ* cell" will be inexpensive, can be easily modified to fit various experimental conditions and types of equipment, and can be manufactured in a decentralized fashion with better quality control than cells with machined parts. This novel cell design will ultimately allow configuration for *ex situ* analysis or *in situ* x-ray diffraction (XRD) spectroscopy. The cell, which in its *ex situ* configuration, is capable of holding a nominal open circuit voltage for twenty-four hours with a loss of 8.6%. Via electrochemical impedance spectroscopy (EIS), it was determined that the cell has an interfacial resistance of ~1800 ohms, unfortunately, higher than that observed in commercial cells. The 3D printed cell, in its *in situ*

configuration, is capable of holding a nominal open circuit voltage for seven hours with a loss of only 0.86%. This work provides the motivation and a roadmap that will spawn the development of a series of "3D-printed *in situ* cells" that can be used as standards in labs globally. Further, this set of standard cells will enable the rapid development of next-generation battery materials.

Acknowledgments

The author would like to thank Dr. Vicky Doan-Nguyen for her guidance and support throughout the project and throughout his undergraduate career. The author would also like to thank Catrina Wilson and Dr. Jerry Gourdin for their advice during the project. Lastly, the author would like to thank NASA and The Ohio State College of Engineering for scholarship funding for the project.

Vita

Education

The Ohio State University

B.S. Mechanical Engineering (2016-2020)

Publications

Goetz, D., "3D-Printed Electrochemical Cell for *In Situ* Analysis" Ohio Space Grant Consortium Annual Research Symposium Proceedings XXVIII.

Goetz, D., Owusu-Antwi, D., & Culbertson, H., "PATCH: Pump-Actuated Thermal Compression Haptics" IEEE Haptics Symposium 2020.

Fields of Study

Major Field: Mechanical Engineering

Minor Field: Computer Information Science

Table of Contents

List of Tables

List of Figures

Chapter 1. Introduction

1.1. Motivation

According to the EPA[1], electricity and transportation contribute to over half of the country's greenhouse gas emissions (Figure 1). Therefore, the adoption of renewable energy into our electrical grid and electric vehicles into our transportation network is essential if we are to reach carbon neutrality. The time-varying output of renewable energy and the portable nature of vehicles necessitate the use of energy storage systems for effective operation. Scientists and engineers have realized the importance of developing these energy storage systems and over the past few decades research into electrical energy storage has grown rapidly[2] (Figure 2). Many of these studies seek to explore novel materials and leverage their unique properties. Thus, it is critical to establish structure-property relationships to develop and evaluate the next generation of higher-performing materials. For battery technology, one way to improve the performance evaluation of the electrode and electrolyte materials is through *in situ* analyses which elucidate the materials' structure-property-performance relationships. For example, there is still limited knowledge about ionic diffusion within the electrolyte and at electrode-electrolyte interfaces of solid-state electrolytes[3]. *In situ* x-ray diffraction (XRD) could be used to analyze these electrolytes to garner a further understanding of ionic diffusion at the interfaces.

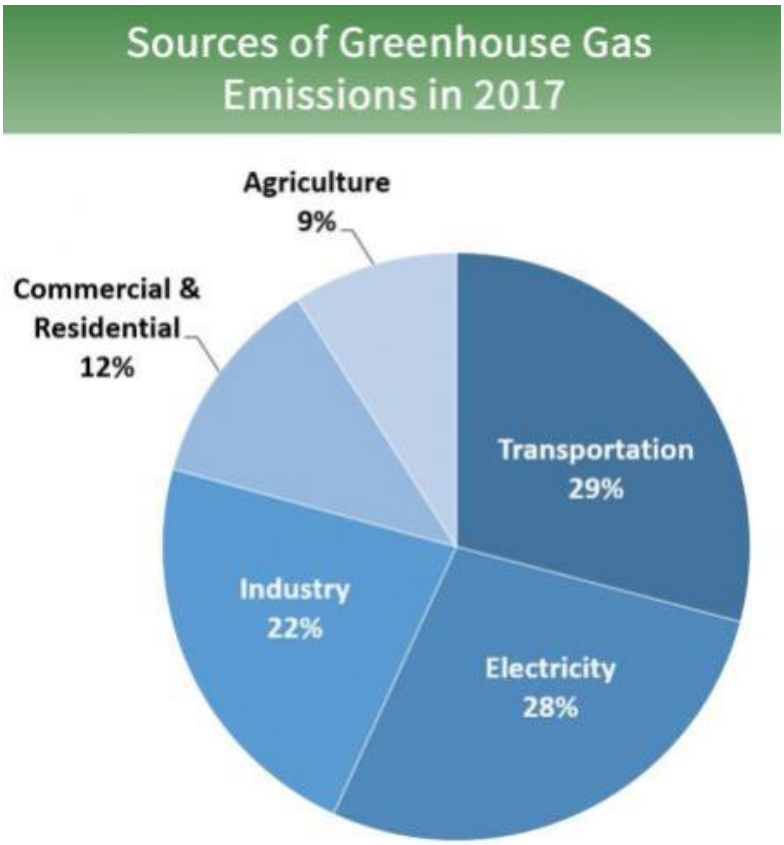

Figure 1: Breakdown of emission from the EPA[1]. Transportation and electricity contribute to 29% and 28% percent respectively. With advancements in energy storage technologies, these two contributions can be decreased drastically.

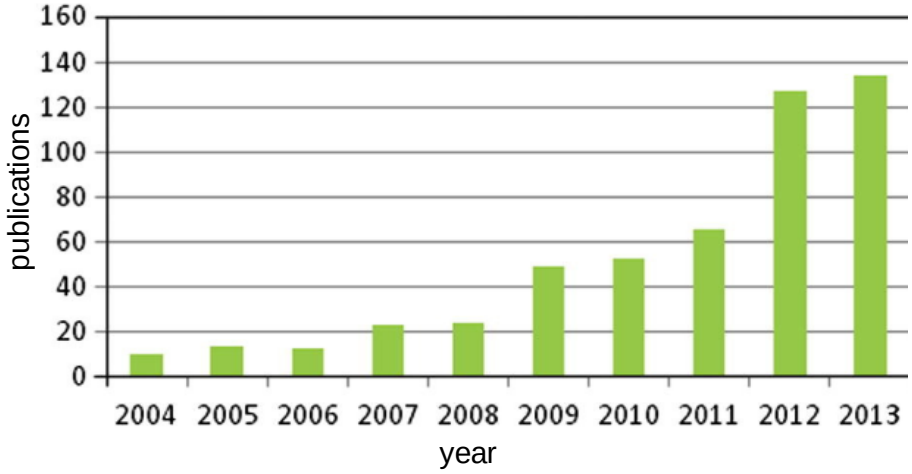

Figure 2: Growth of research in electrical energy storage systems[2].

To conduct *in situ* XRD tests on battery components, the battery stack must be contained in a cell with a window that x-rays can penetrate. Unfortunately, these cells are relatively expensive, with commercial single-use cells costing around $25 and commercial reusable cells costing up to $2,000[4]. These costs have led individual labs to develop their own *in situ* XRD cells[5,6] or to modify inexpensive coin cells[7]. Figure 3 shows the development of *in situ* cells during the last half century. Because various cells have been developed by different groups, often for unique applications, the electrochemical landscape has been fragmented, with different studies being conducted with different cells[8]. Furthermore, these cells are not commercially available, meaning that groups wanting to use these cells must individually manufacture them, often involving machining of custom parts. Decentralized manufacturing of cells and modification of commercial cells may lead to low quality control. The lack of a standard cell makes the comparison of results between labs difficult and could inhibit the development of novel electrochemical materials.

Creating a singular cell for XRD *in situ* analysis is a daunting task due to different experimental setups in each lab (different spectrometers, sample holders, and X-ray collection modes as well as different reactivity of the battery components being analyzed)[8]. Thus, if a standardized cell design is to be created, it should take inspiration from Borkiewicz, et al.'s AMPIX cell and prioritize versatility[6].

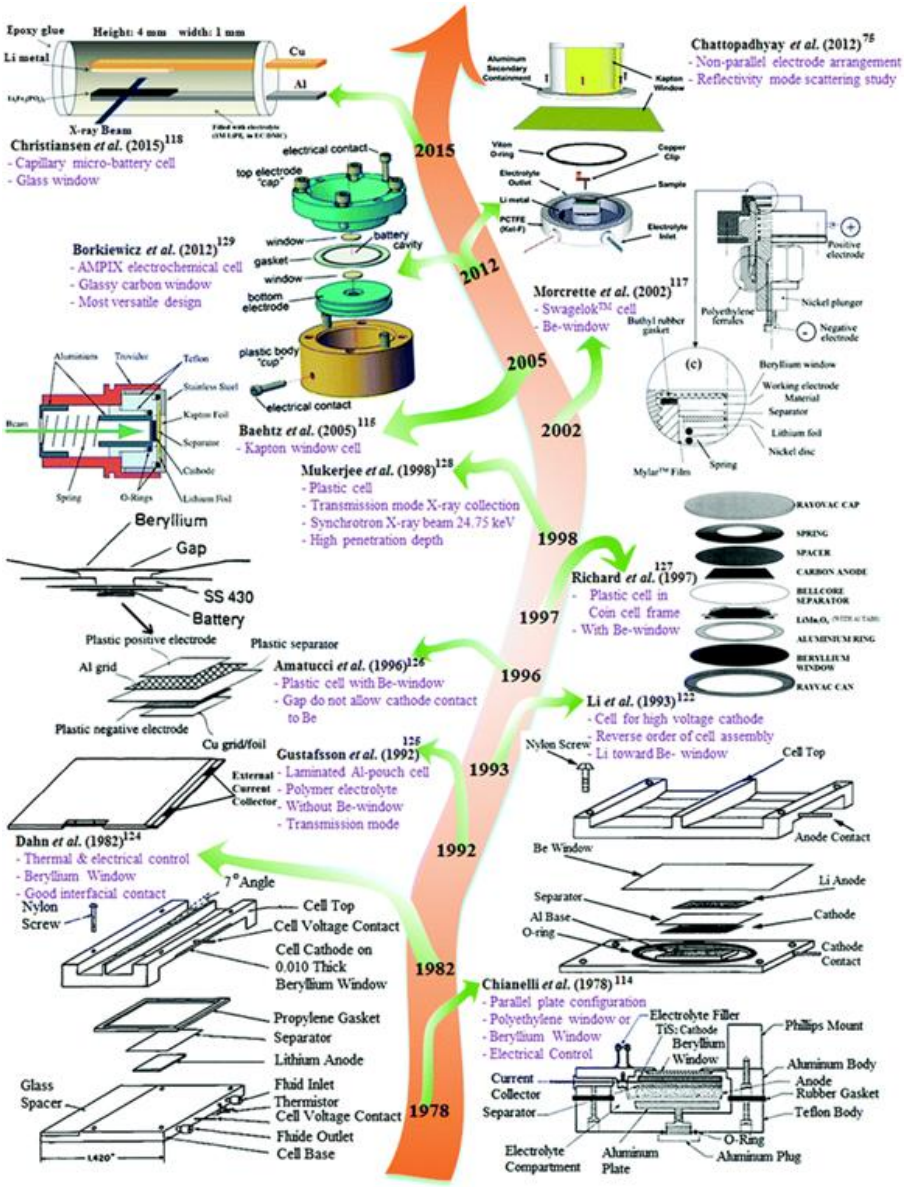

Figure 1: *In situ* cells that have been developed by labs over the last half century[9]. Many of these designs are difficult to manufacture or modify because they have custom machined parts.

1.2. Proposed Solution

In an effort to standardize *in situ* cells across labs, we designed an *in situ* cell that is constructed entirely from 3D-printed and commercial components. Whereas other *in situ* cell

designs have machined parts, recent developments in 3D-printing technologies allows an alternative route of cell design. By downloading CAD files for 3D-printing and ordering common components from vendors, individual labs can assemble and use *in situ* cells that are identical to those in other labs without machining custom parts or paying the high costs for commercial cells. Furthermore, individual labs can make modifications to the CAD files depending on their experimental conditions. These modified CAD files can then be re-uploaded to share with the research community. It is envisioned that there will be an online repository with cell designs uploaded by researchers, each optimized for different experimental conditions. Each cell design will include CAD files, assembly instructions, and links to commercial components. To demonstrate the feasibility of this approach, we created and tested an *in situ* XRD cell that is constructed entirely from 3D-printed and common commercial components.

Chapter 2: Methodology

2.1. Design Requirements

The cell has two main functions: to allow cycling of the battery and to allow the battery material (electrodes and electrolyte) to be observed using various spectroscopy techniques. To allow for cycling, housing is needed to hold the battery stack. This housing must be impervious to both air and the electrolyte fluid. Furthermore, conductive probes must be connected to the anode and cathode to provide a channel for electrons to flow during cycling. Pressure should also be applied to maintain solid contact between the separator and electrodes the cell. Materials for the cell housing and probes should be selected as to not react with the battery materials. To allow for *in situ* observation of the battery materials, it is necessary to have an opening in the housing that is covered by a cell window. The material for this window should be selected for the specific spectroscopy technique so that is does not interfere with the spectrometer's beam. For spectrometers in transmission mode, a window is needed for both the top and bottom of the cell, whereas for spectrometers in reflection mode, a window is only needed on the top of the cell.

2.2. Initial Designs

The cell design underwent multiple iterations as features were added to improve performance. There were four main groups of prototypes that were designed. All designs used 3D-printed material for the housing and common, "off-the-shelf" parts for the other cell

components. Bolts and wingnuts were used to clamp the two halves of the cell battery together to apply pressure to the battery stack.

The first group of prototypes were completely symmetric designs with the top and bottom parts of the housing having cavities of equal depth. This prototype was designed so that conductive windows could be used as current collectors for cycling the cell. Stainless steel washers and a wave spring were added to maintain conductivity to the battery stack and provide pressure to the cell. Figure 4 shows the top/bottom of one of the designs for the first group of prototypes.

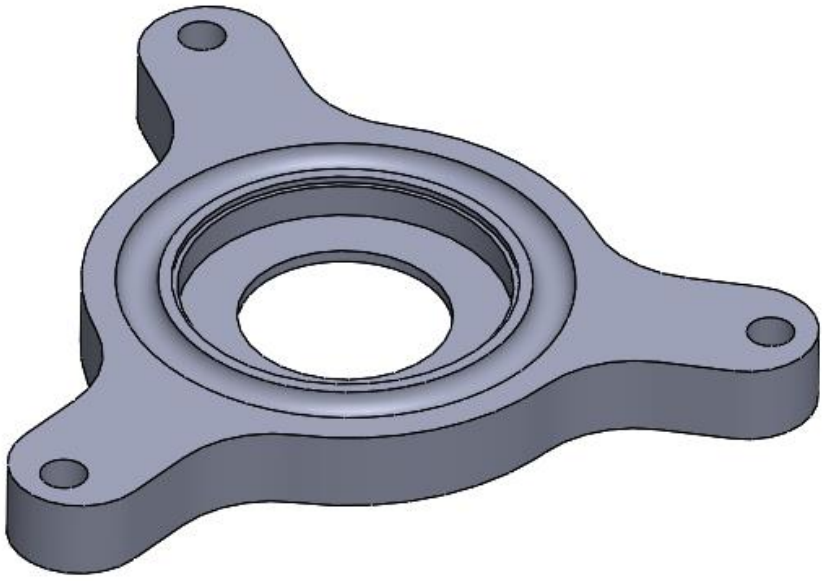

Figure 4: This is one of the CAD models for the design of the first group of prototypes. This design is used for both the top and bottom of the cell housing.

The second group of cell designs had two major modifications from the first designs. Firstly, the bottom housing of the cell was designed to have a deeper cavity than the top housing of the cell to allow for easier assembly. This design change also better matches the asymmetrical nature of the cell components (i.e. there is a spring on one side of the battery stack that applies

pressure through the cell). Secondly, slots were added to the side of the housing to allow for shims to contact the washers. This allows for conductivity through the shims instead of through the window, eliminating the requirement for the window to be conductive. This also means that the window can be moved to the outside of the cell housing which makes the assembly process easier. Furthermore, having the electrical leads on the side instead of the top makes it less likely for interference between the leads and the spectrometer beam.

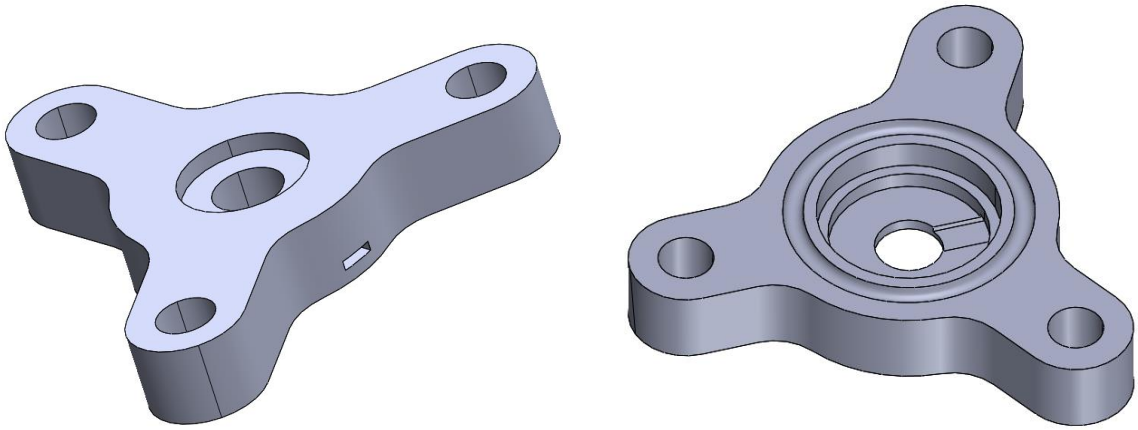

Figure 5: Set of CAD models for the design of the second group of prototypes. The cell top is shown on the left and the cell bottom is shown on the right.

The next major change for the design was that covers (specific to the window dimensions) were added to the top and bottom of the cell. This third group of prototypes was more modular because by simply exchanging the covers and windows, the cell can be purposed for various types of spectroscopy techniques. A cell cover without an opening can be added and the window can be removed to cycle the cell and conduct *ex situ* analysis. In this *ex situ*, configuration, the washers are replaced with spacers (solid disks) to achieve a more uniform pressure profile. Additionally, these prototypes were the first group tested experimentally, so the dimensions of the design were tuned to achieve tighter tolerancing between 3D-printed

components and commercial components (e.g. washers, springs, shims). The design for this group of prototypes is shown in Figure 6 and the fully assembled cell is shown in Figure 7.

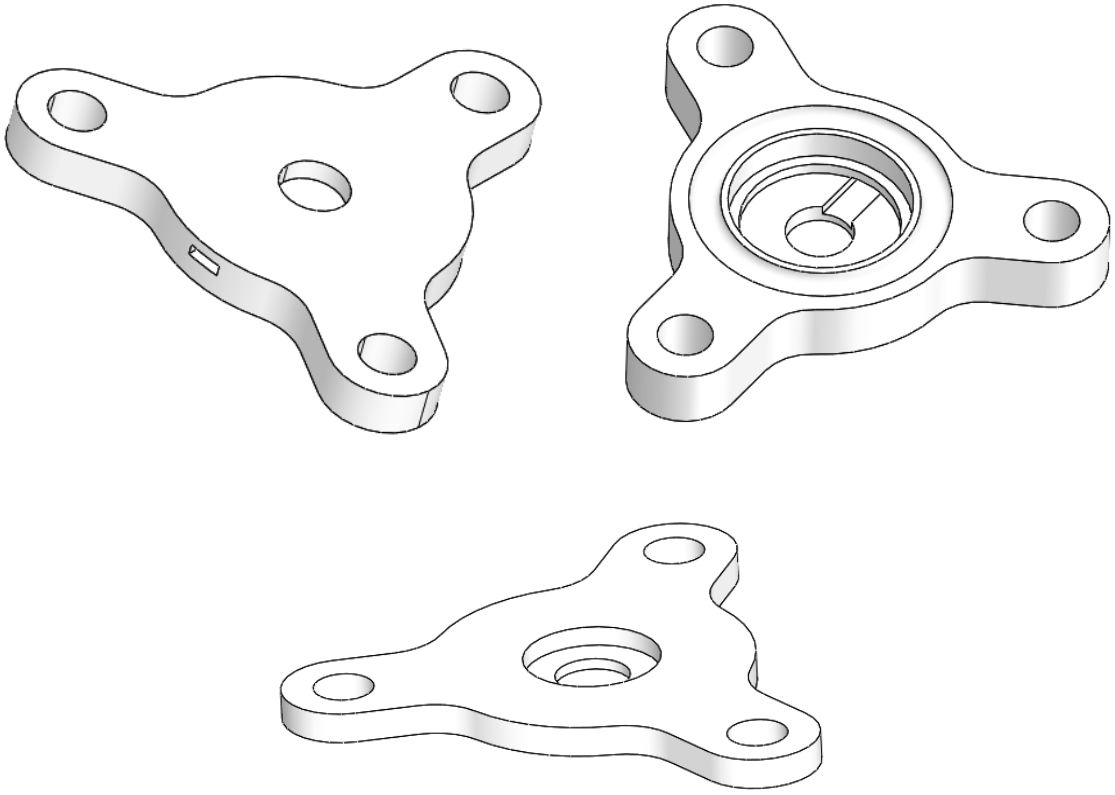

Figure 6: Set of CAD models for the design of the third group of prototypes. The cell top, cell bottom, and cell cover are shown on the left, right, and bottom respectively. The cell cover is used on both the top and bottom of the cell. The cover pictured here is for a graphite window.

Figure 7: Third prototype assembled. This cell is assembled in a configuration for *ex situ* testing.

Because many battery components react with the oxygen or the humidity in air, the cell should be assembled in an inert environment (i.e. a glovebox). This means that the person assembling the cell is usually wearing multiple pairs of gloves which reduces dexterity significantly. Therefore, ease of assembly was a priority during the cell design. To further aid the assembly process, an assembly stand was designed and 3D-printed (Figure 8).

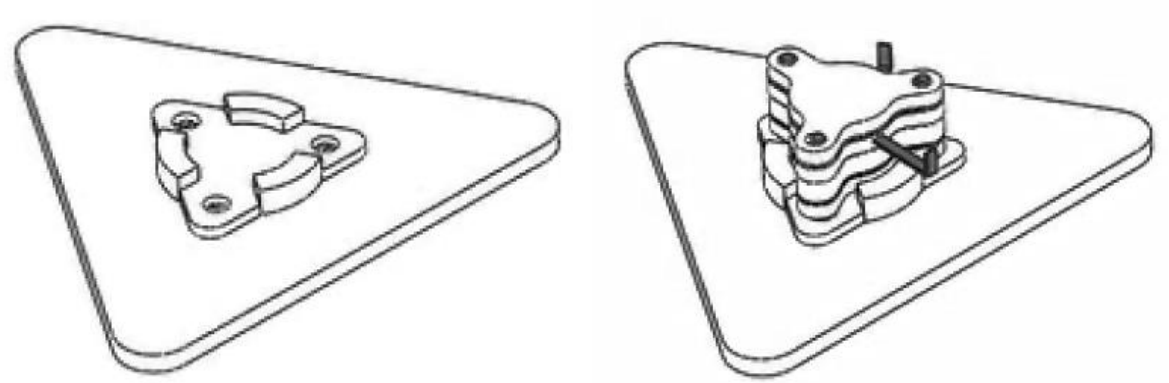

Figure 8: Assembly stand. On the left is a CAD model of the assembly stand and on the right is a CAD model of the third cell prototype being assembled with the stand. The stand was 3D-printed and used to ease the assembly process.

2.3. Final Design

The designs for the cells for the first three sets of prototypes were for operation in transmission mode, meaning that the spectrometer measures the beams that pass through the materials. In transmission mode, the spectrometer detector is placed opposite of its emitter, so two cell windows are needed to allow the beam to pass completely through the cell. The fourth and final design was modified for operation in reflection mode. In reflection mode the spectrometer detector is placed at an angel from its emitter to measure reflected beams. In this setup, only one cell window is necessary. Therefore, the bottom cover and bottom window was

removed from the design and the bottom washers were replaced with spacers. The cell architecture is shown in Figure 9.

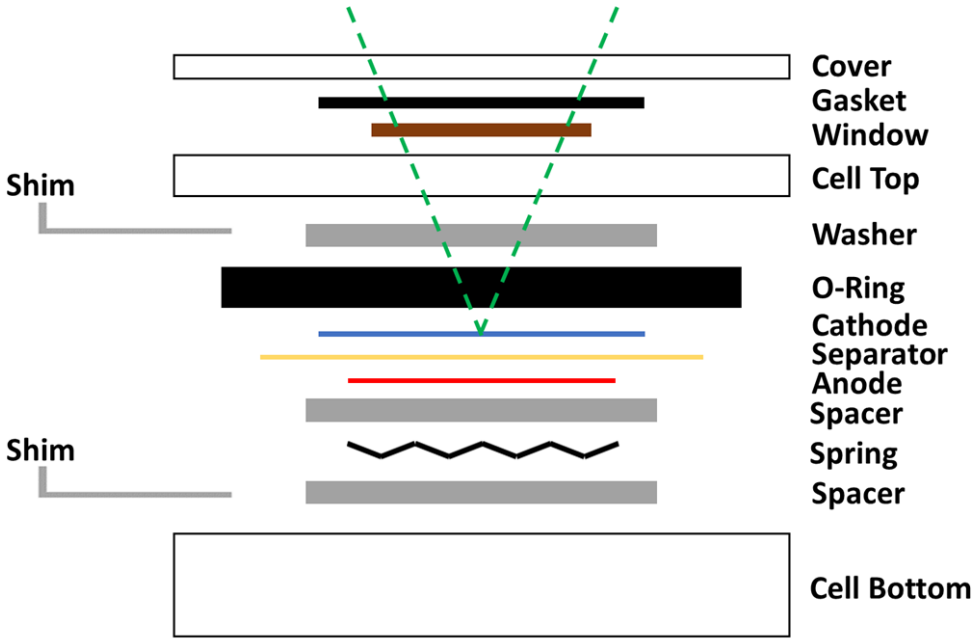

Figure 9: Architecture of the fourth cell prototype. The green dashed line represents the spectrometer beam in reflection mode.

Like previous *in situ* cell designs, the cell was designed to operate with a reflection angle up to 100 degrees. To achieve this angle and prevent interference with the spectrometer beam, some of the components were enlarged from the previous designs. The minimum necessary diameters of components were calculated using Equation 1. Components larger than the minimum dimensions were selected and their factors of safety were calculated using Equation 2. The result from the calculations are tabulated in Table 1. A positive byproduct of enlarging components is that it makes the assembly process easier.

Equation 1: $Minimum\ Necessary\ Diameter = 2 * \frac{Distance\ from\ Top\ of\ Part\ to\ Material}{\tan(40^0)}$

Equation 2: $Factor\ of\ Safety = \frac{Diameter\ of\ Selected\ Component}{Minimum\ Necessary\ Diameter}$

Table 1: Dimension constraints. This table shows the minimum necessary diameters of various components to avoid interference with the spectrometer beam. It also shows factors of safety for the selected components.

Component	Thickness (in)	Mininum Diameter (in)	Actual Diameter (in)	Factor of Safety
Washer	0.055	0.131	0.281	2.144
Cell Top	0.07	0.298	0.310	1.040
Window	0.0033	0.306	0.591	1.931
Gasket	0.072	0.477	0.490	1.026
Cell Cover	0.05	0.597	0.610	1.022

Figure 10 shows the prototype of the cell and the paragraph below provides further details about the cell design. The cell has stainless steel washers (McMaster-Carr 90107A029) on top of the battery stack and a spacer (MTI CR20SPA02) beneath the stack for electrical conductivity. A stainless-steel wave spring (MTI CR20WS-SPR) is beneath the bottom spacer of the stack. The spring is used to maintain pressure in the cell and maintain conductivity between the spacer in the stack and another spacer beneath the spring. These components are housed inside of the 3D-printed cell top and bottom with an O-ring (Grainger 1CRW4) as a seal. There is an opening in the cell top to allow for the X-rays to reach the stack. Stainless-steel shims (McMaster-Carr 8836A11) protrude from slots in the sides of the cell top and bottom. These shims are in contact with the top and bottom washers and act as current collectors that can be used to cycle the cell. A cell window, in our case Kapton (Grainger 15C543), is placed over the opening in the cell top. A 3D-printed cell cover, also with an opening, is positioned on to the window to hold it in place and a gasket (McMaster-Carr 91367A925) is used as a seal. The whole assembly is held together by three bolts (Grainger 2EB77) that run through the 3D-printed

components and wingnuts (McMaster-Carr 90866A009) are used to tighten the cell, compressing the spring.

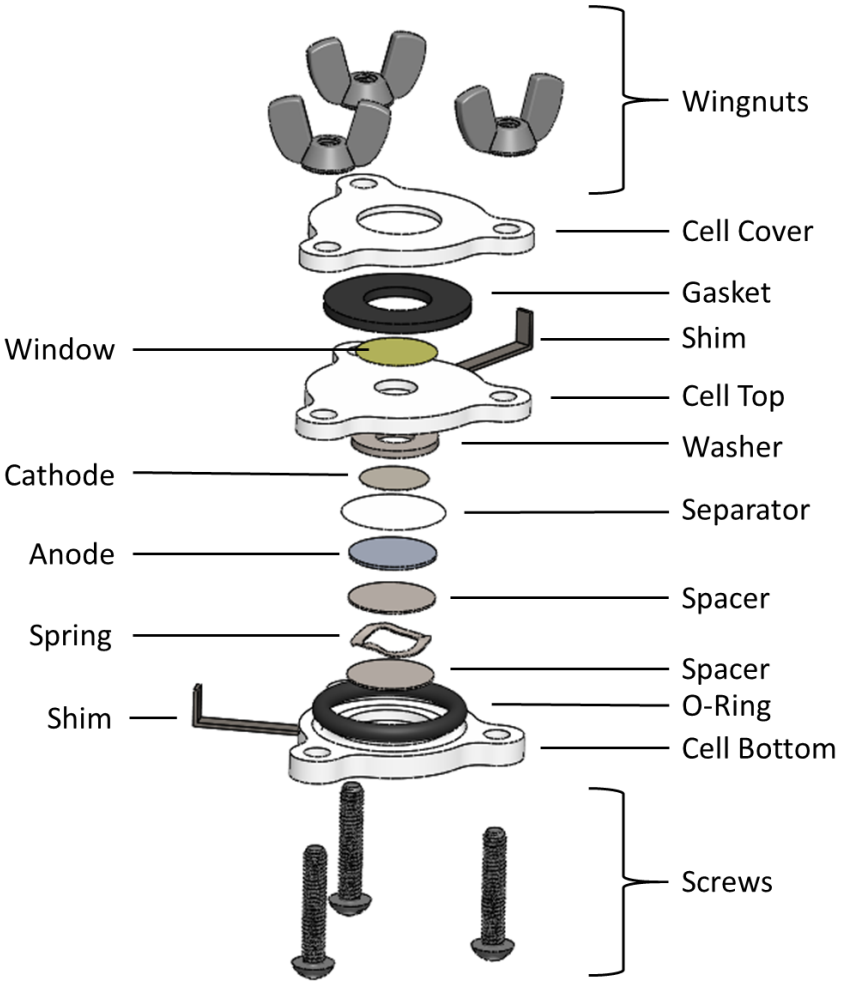

Figure 10: CAD model showing exploded view of the final cell prototype.

The 3D-printed components were created using stereolithography (SLA) printing. This method is preferable to fused deposition modeling for our application because parts created through SLA printing generally have higher precision and are impervious to the electrolyte fluid and air. An Anycubic Photon 3D-printer and 405 nm UV resin was used to print the components. Using the cost of UV resin and the cost of commercial components, a cost analysis was

conducted on the cell. The cell was calculated to cost $13.82 and is broken down in more detail in Table 2.

Table 2: Cell cost analysis. This table shows the cost per component and total cost of the cell. The cost for 3D-printing was determined by the volume of the part and the cost of UV resin.

Parts	Quantity	Cost Per Unit	Vendor
Springs	1	$ 0.60	MTI
Spacers	2	$ 0.49	MTI
Washers	1	$ 0.08	McMaster
Bolts	3	$ 0.03	Grainger
Wing Nuts	3	$ 0.09	McMaster
Shims	2	$ 4.49	McMaster
O-rings	1	$ 0.06	Grainger
Gasket	1	$ 2.13	McMaster
Bottom	1	$ 0.18	3D-Printed
Cover	1	$ 0.10	3D-Printed
Top	1	$ 0.13	3D-Printed
Window	1	$ 0.22	Grainger
Total:		**$ 13.82**	

2.4. Experimental Setup

To verify that the 3D-printed material was impervious, leak tests were conducted with 3D-printed components and water. Two bowl-shaped components were printed and weighed. A dry piece of paper was placed between the two components and they were clamped together with a silicon gasket seal. The components were then completely submerged in 40 mL of water. After 48 hours, the paper was checked for dampness and the components were re-weighed after drying in the vacuum oven.

For all the electrochemical testing, the cell held a lithium-based battery stack. A lithium chip was used as the anode and $LiCoO_2$ was used as the cathode. 60 μL of 1.0 M $LiPF_6$ in EC/DMC was used as the electrolyte and a polypropylene Celgard was used as the separator. The battery stack was assembled with the cathode on top so that it could be viewed through the cell window.

Electrochemical tests were conducted on the cell both in its configuration for *ex situ* analysis and for *in situ* analysis (configurations shown in Figure 11). In the *ex situ* configuration, the window was removed, and the washer was replaced with a spacer. Initially, open circuit voltage (OCV) tests were conducted on both cell configurations. During these tests, the cell was assembled and the open circuit voltage (potential difference) between the two current collectors (shims) was measured over twenty-four hours in the glovebox. Electrochemical Impedance Spectroscopy (EIS) tests in the glovebox were also conducted on the cell in *ex situ* configuration to obtain information regarding the interfacial resistance in the cell.

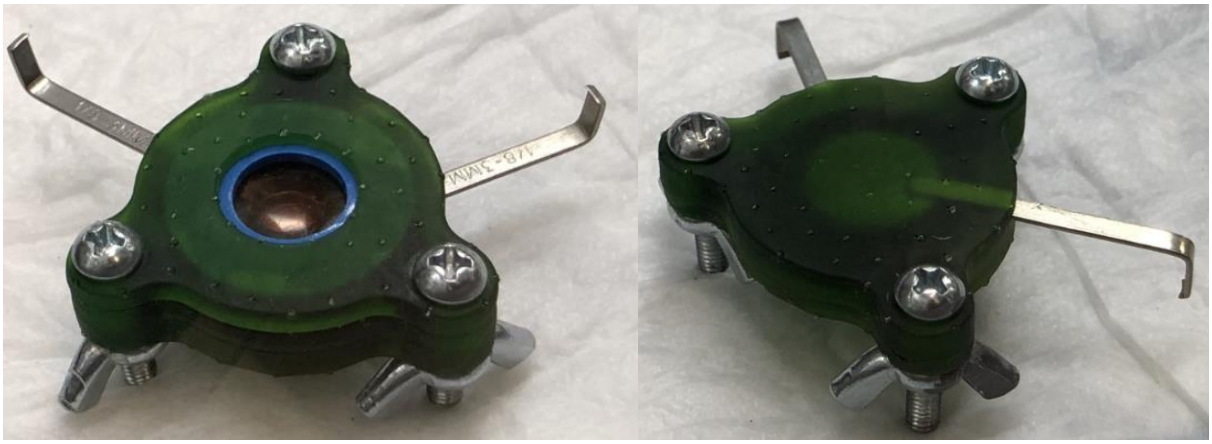

Figure 11: (Left) *In Situ* Configuration of Cell. (Right) *Ex Situ* Configuration of Cell. This shows the setup for the cells from the fourth set of designs.

Chapter 3: Results and Analysis

3.1. Leak Test Results

After being submerged for 48 hours, the piece of paper encased in the 3D-printed parts was still dry. Furthermore, the parts only gained 0.01345 g (0.74% of its mass) after being submerged for 48 hours. Other leak tests were also conducted, but this result was the most definitive in showing that the material is impervious to water for prolonged periods. The material's non-porous nature makes it a viable selection for use in the cell design.

3.2. Open Circuit Voltage Test Results

Twenty-nine OCV tests were conducted over the past year and a half (23 with the 3D-printed cell and 6 with a commercial cell). The OCV test results from the commercial cell (MTI HSTC20) were used as baseline measurements for comparison to the 3D-printed cell data.

Each OCV test was categorized into one of four groups: 1) successful, 2) low OCV, 3) immediate short, or 4) break in connection. Group 1 consisted of tests in which the cell initially displayed voltage in the desired range (close to 3.4 V versus Li/Li^+) and stayed in this range for the duration of the 24-hour rest period. Group 2 consisted of tests in which the cell's OCV dropped well below the desired voltage either immediately or during the 24-hour rest period. Group 3 consisted of tests in which the cell immediately displayed an OCV close to zero, indicating that the cell had shorted. Group 4 consisted of tests in which the cell had an infinite

OCV meaning that there was a break in the connection between two of the metal components in the cell. An overview of the all 29 OCV tests and their categorizations are shown in Figure 12.

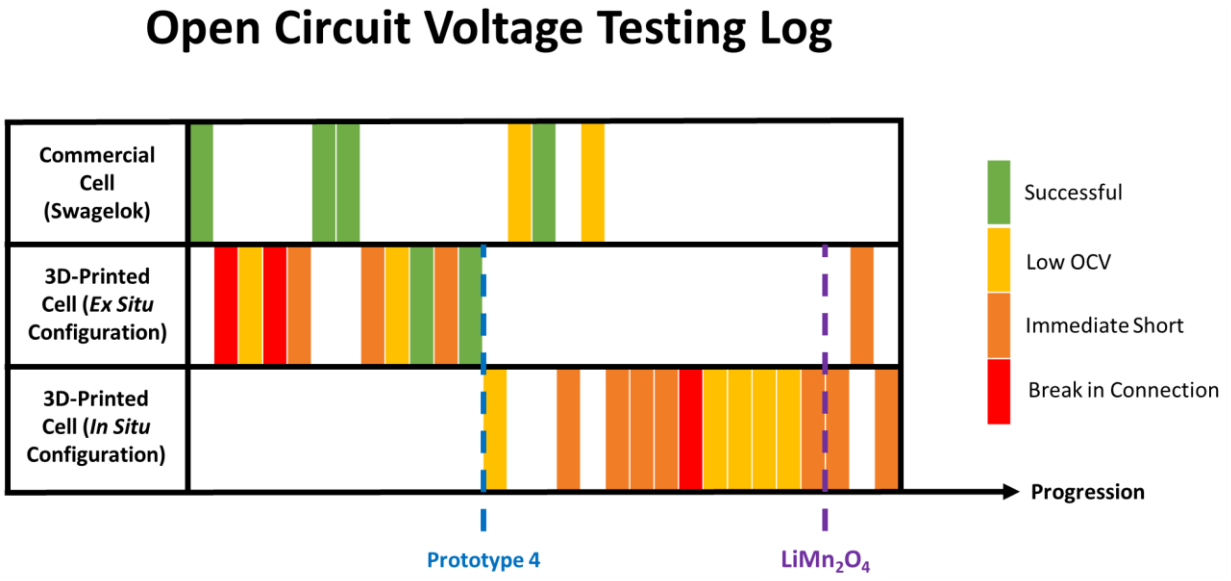

Figure 12: Overview of OCV testing progression from past year and a half. The green rectangles indicate the successful tests (Group 1). The yellow rectangles indicate tests in which the cell had a low OCV (Group 2). The orange rectangles indicate tests in which a short occurred immediately (Group 3). The red rectangles indicate tests in which there was a break in connection in the cell. The blue dashed line indicates the switch from prototype 3 to prototype 4 and the purpled dashed line indicates the switch from $LiCoO_2$ to $LiMn_2O_4$ for the cathode material.

Overall, 6 out of 29 tests (21%) were successful. Of these 6 successful results, 4 were from the commercial cell and 2 were from the 3D-printed cell (both in its *ex situ* configuration). Overall, 4 out of 6 tests (67%) with the commercial cell were successful whereas only 2 of 23 tests (9%) with the 3D-printed cell were successful. 2 out of 10 tests (20%) were successful for the 3D-printed cell in its *ex situ* configuration, whereas 0 out of 13 tests (0%) were successful for the 3D-printed cell in its *in situ* configuration.

The inconsistent results from the 3D-printed cell were likely due to the more cumbersome assembly process. The modular design of the 3D-printed cell increases the number

of components necessary for assembly. Furthermore, the commercial cell has the top and bottom pieces threaded to allow for them to be easily screwed together, whereas the 3D-printed cell has three separate bolts that must be tightened individually. Designs were explored with 3D-printed threaded top and bottom, but tolerancing limitations and the brittleness of the 3D-printed material made this design infeasible.

The profiles of the six OCV tests that were successful are shown in Figure 13. Overall, during successful tests, the 3D-printed cell and commercial cell had similar OCV profiles. The average loss in OCV over 24 hours was 5.9% for the commercial cell and 8.6% for the 3D-printed cell.

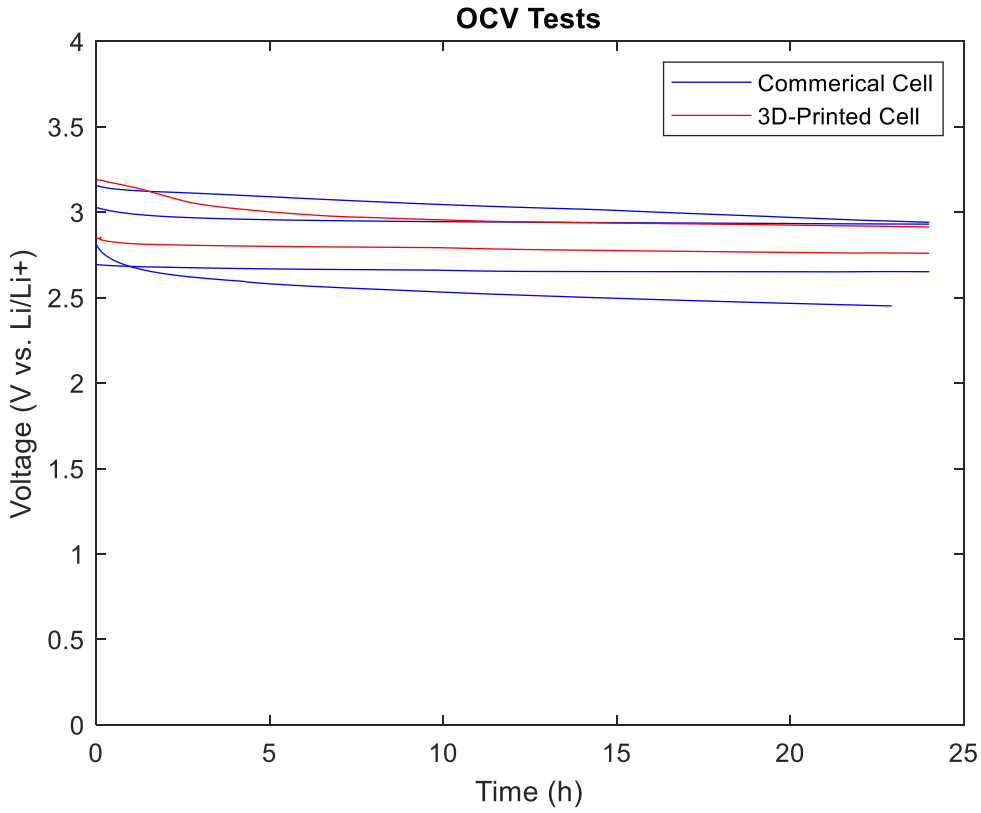

Figure 13: OCV profiles. The blue lines represent the OCV profiles of the commercial cell. The red lines represent the OCV profiles of the 3D-printed cell (in its *ex situ* configuration).

There were two major modifications to the OCV tests over the past year and these are marked by dashed lines in Figure 12. One modification was that the cathode material was changed from $LiCoO_2$ to $LiMn_2O_4$. The other modification was that the cell design was changed from prototype 3 to prototype 4. This modification was made for a few reasons. Firstly, prototype 4 has a shallower cavity for the battery stack than prototype 3, allowing an increase in compression of the spring resulting in increased pressure. Secondly, prototype 4 is configured for spectrometer in reflection mode instead of transmission mode, reducing the number of components in the assembly, making the assembly less cumbersome. Lastly, prototype 4 was designed to fit the windows and gaskets in lab so it could be assembled in its *in situ* configuration (washer in place of top spacer and cover with cavity for window and gasket).

Only three tests were conducted after the cathode material was changed so it is difficult to determine if this influenced the tests. It is surmised that this change did not affect the results since both materials are common cathodes. The change from prototype 3 to prototype 4 (coinciding with changing the cell configuration from *ex situ* to *in situ*) does appear to affect the OCV test results. The percentage of time that the cell shorted immediately upon assembly increased from 33% to 57%. The percentage of time that the cell had low OCV values also increased from 22% to 36%. The increased pressure in the cell due to the design changes coupled with the change from a spacer to a washer for the top current collector could cause an increase of force on regions of the battery stack. This increased force, in turn, may cause damage to the separator resulting in more shorts.

Although the OCV tests with prototype 4 yielded no successful results, some of the resulting OCV profiles showed promising signs. Two of the tests initially showed the desired

voltage but decreased steadily to around an OCV value of 1 V after 24 hours. The most promising test initially showed the desired voltage and held this value for 7 hours before shorting. The profile for the first 7 hours of this test is shown in Figure 14.

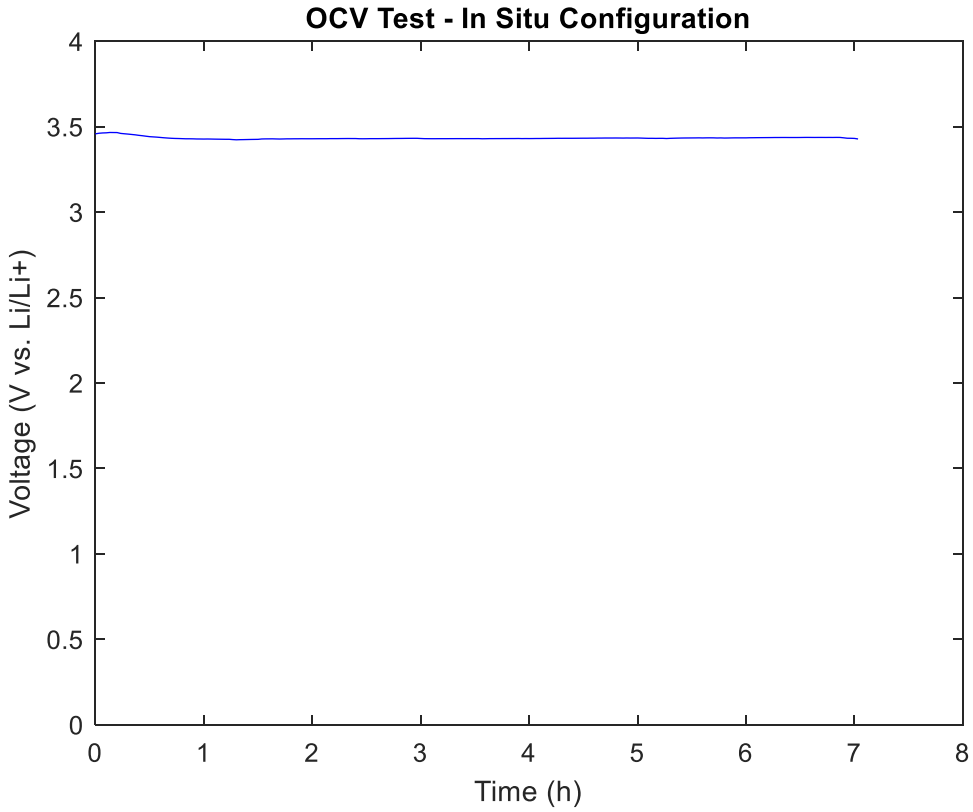

Figure 14: OCV profile for first 7 hours of promising test. The 3D-printed cell used the design from prototype 4 and was assembled in its *in situ* configuration.

3.3. Electrochemical Impedance Spectroscopy Results

Some of the cells that had successful OCV results underwent EIS testing. For the EIS tests, the frequency was scanned from 1000 kHz to 50 mHz with 10 points per decade sampling. The input voltage had an amplitude of 100 mV. The results from the EIS for prototype 3 of the 3D-printed cell and the commercial cell can be seen in Figure 15.

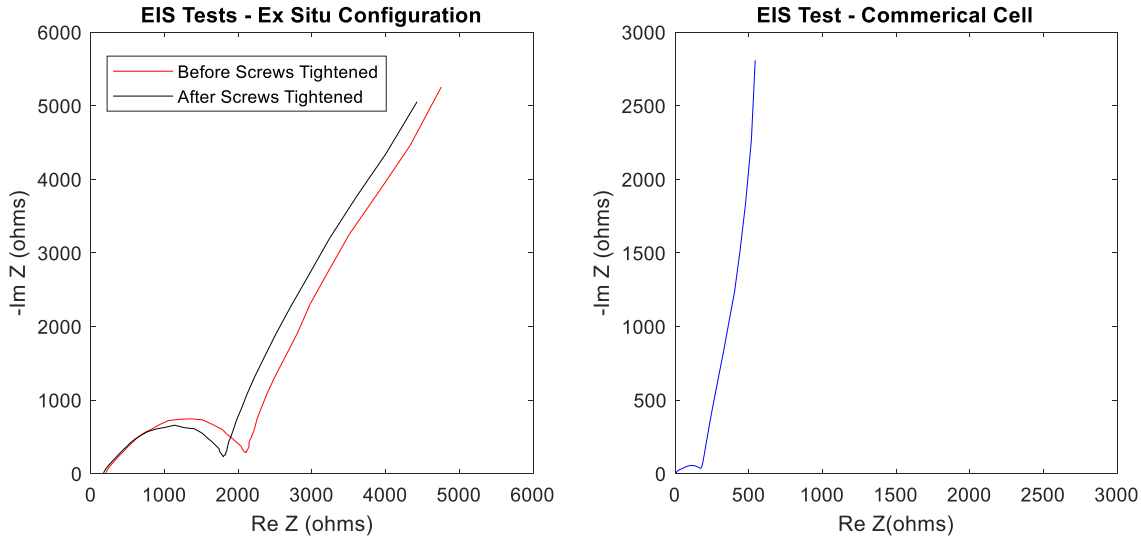

Figure 15: (Left) EIS data for 3D-printed cell in its *ex situ* configuration. (Right) EIS data for commercial cell. The EIS data shows that there is about 10 times more interfacial resistance in the 3D-printed cell compared to the commercial cell.

The y-intercept of the graph shows the baseline resistance in the cell. The "elbow" of the graph shows the amount of interfacial resistance in the battery stack. For the commercial cell, there is a baseline resistance of ~40 ohms and an interfacial resistance of ~180 ohms. For the 3D-printed cell there is a baseline resistance of ~175 ohms and an interfacial resistance of ~2,100 ohms. The bolts on the 3D-printed cell were tightened further and another EIS test was conducted. The interfacial resistance decreased to ~1,800 ohms.

The higher baseline resistance in the 3D-printed cell is likely due to the extra metal components that the current must flow through to reach the battery stack in the 3D-printed cell. The commercial cell also likely has current collectors that were manufactured to have low resistance, whereas generic shims were used in the 3D-printed cell. There are a few factors that likely contributed to the high interfacial resistance in the battery stack. Firstly, the cell likely did not have adequate pressure, causing a less than ideal interface between the battery components. This was one of the main reasons that the cavity size was decreased in prototype 4. Although this

theory is supported by the fact that tightening the bolts of the cell decreased the interfacial resistance, it is unlikely that it is the only cause. Evaporation of the electrolyte fluid or uneven pressure distributions could have also contributed to the high interfacial resistance.

Chapter 4: Conclusion

4.1. Summary

In conclusion, the cell showed potential to be the first 3D-printed cell in a set of standardized *in situ* cells. The cell, although inconsistent, demonstrated the ability to hold an OCV over a 24-hour period with similar loss rates to a commercial cell. The cell had much larger interfacial resistance than the commercial cell. The cell can be produced for a fraction of the cost of other reusable *in situ* cells and has a modular decision that can easily be modified by the user. It is envisioned that the design and assembly procedures can be distributed to labs globally through a repository such as GrabCAD. Because all parts are 3D-printed or common commercial components, it will be easy for researchers to print and assemble their own cells and conducts experiments with the same standard cells as other labs.

4.2. Next Steps

The immediate next steps for the project are to determine the causes for inconsistent OCV results and work towards reducing the interfacial resistance of the cell. Exploring assembly with multiple layers of separators could help to provide more protection against separator damaging. Increasing pressure in the cell will hopefully reduce the interfacial resistance and perhaps adding more electrolyte fluid could help ensure that evaporation doesn’t cause the electrodes to become dry.

After these issues are addressed, cycling of the cell in the glovebox should be conducted to observe its performance. Then *in situ* XRD should be conducted to show its performance outside of the glovebox in an *in situ* environment.

4.3. Future Work

An interesting study that could be conducted as a follow up to this work would be a thorough exploration of the effect of pressure on interfacial resistance. Using current collectors of various shapes and different magnitudes of pressure, changes in the EIS profiles could be analyzed to determine resistances in the cell. Furthermore, models could be created relating pressure distributions to interfacial resistance, hopefully finding minima that reduce resistances in cells. This could lead to a longer cycle life of battery cells.

Another potentially impactful follow-up study would be the creation of an array of 3D-printed *in situ* cells. Due to the low cost of 3D-printed *in situ* cells, an array of hundreds of cells could be printed allowing for rapid analysis of novel materials. A 3D-printer could potentially be designed to print all components of the cell including the battery stack. This could eventually lead to a closed loop system that autonomously synthesizes and tests new materials.

Bibliography

[1] "Inventory of U.S. Greenhouse Gas Emissions and Sinks 1990-2017," Tech. Rep. (EPA, 2019).

[2] Luo, M. Dooner, and J. Clarke, "Overview of current development in electrical energy storage technologies and the application potential in power system operation," Applied Energy (2014)

[3] K. Kerman, A. Luntz, V. Viswanathan, Y.-M. Chiang, and Z. Chen, "Review - Practical Challenges Hindering the Development of Solid State Li Ion Batteries,"164, A1731–A1744 (2017).

[4] MTI Corporation, "Battery R&D Equipment," (2020).

[5] J. Sottmann, V. Pralong, N. Barrier, and C. Martin, "An electrochemical cell for operando bench-top X-ray diffraction," Journal of Applied Crystallography 52, 485–490 (2019).

[6] O. J. Borkiewicz, B. Shyam, K. M. Wiaderek, C. Kurtz, P. J. Chupas, and K. W. Chapman, "The AMPIX electrochemical cell: a versatile apparatus for in situ X-ray scattering and spectroscopic measurements," Journal of Applied Crystallography 45, 1261–1269 (2012).

[7] M. N. Richard, "A cell for in situ x-ray diffraction based on coin cell hardware and bellcore plastic electrode technology," Journal of The Electrochemical Society 144, 554 (1997).

[8] M. Morcrette, Y. Chabre, G. Vaughan, G. Amatucci, J. B. Leriche, S. Patoux, C. Masquelier, and J. M. Tarascon, "In situ x-ray diffraction techniques as a powerful tool to study battery electrode materials," Electrochimica Acta 47, 3137 – 3149 (2002).

[9] A. Tripathi, W. Su, B. Hwang. "In situ analytical techniques for battery interface analysis," Chemcial Society Review 47, 736-851 (2018).